ORIGINAL PAPER

Micelles obtained by aggregation of gemini surfactants containing the CCK8 peptide and a gadolinium complex

Antonella Accardo · Diego Tesauro · Anna Morisco · Gaetano Mangiapia ·
Mauro Vaccaro · Eliana Gianolio · Richard K. Heenan · Luigi Paduano ·
Giancarlo Morelli

Abstract Two gemini surfactants, [C18CysL5CCK8]$_2$ and [C18CysDTPAGlu]$_2$, containing, respectively, the CCK8 peptide and the DTPAGlu chelating agent or its gadolinium complex have been prepared by linking lipophilic chains through a disulfide bond between two cysteine residues. The two surfactants aggregate in water solution forming pure or mixed micelles, with a critical micellar concentration in the 5×10^{-6}–5×10^{-5} mol kg^{-1} range, as measured by fluorescence spectroscopy. As indicated by small-angle neutron scattering, the shape and size of the micelles are influenced by the temperature: increasing temperature leads to progressive reduction of the size of the supramolecular aggregates. Cylindrical structures found at lower temperatures (10–40 °C) evolve into ellipsoidal micelles at 50–80 °C. Furthermore, the surface-exposed CCK8 peptide changes its conformation above a transition temperature of approximately 45 °C, going from a β-sheet to a random-coil structure, as indicated by circular dichroism measurements. The mixed aggregate obtained by coaggregation of the two gemini-based amphiphilic compounds, [C18CysDTPAGlu(Gd)]$_2$ and [C18CysL5CCK8]$_2$ in 70:30 molar ratio, represents the first example of a peptide-containing gemini surfactant as a potential target-selective contrast agent in MRI. In fact, it presents a high relaxivity value of the gadolinium complex, 21.5 mM^{-1} s^{-1}, and the CCK8 bioactive peptide exposed on the external surface is therefore capable of selective targeting of the cholecystokinin receptors.

A. Accardo · D. Tesauro · A. Morisco · G. Morelli (✉)
Department of Biological Sciences and IBB CNR,
CIRPeB, University of Naples "Federico II",
Via Mezzocannone 16,
80134 Naples, Italy
e-mail: gmorelli@unina.it

G. Mangiapia · M. Vaccaro · L. Paduano (✉)
Department of Chemistry CSGI—Consorzio Interuniversitario
per lo Sviluppo dei Sistemi a Grande Interfase,
University of Naples "Federico II",
Via Cynthia, 80126 Naples, Italy

E. Gianolio
Department of Chemistry I.F.M.,
Molecular Imaging Centre,
University of Turin,
Via Nizza 52, 10125 Turin, Italy

R. K. Heenan
ISIS-CLRC, Rutherford Appleton Laboratory,
Chilton, Oxfordshire OX11 0QX, UK

Introduction

Over the past two decades magnetic resonance imaging (MRI) has evolved into one of the most versatile and efficient noninvasive tools for clinical diagnosis [1, 2]. The advent of high magnetic fields, improved gradient coils, and pulse sequences has provided the means to obtain three-dimensional images of the internal part of the body at near cellular resolution [3]. The resolution of the image can be improved by administration of contrast agents. Stable complexes of gadolinium ion with polyaminocarboxylate ligands have been extensively used as paramagnetic contrast agents for MRI [4], because of their high

paramagnetism (seven unpaired electrons) and because of their favorable properties in terms of electronic relaxation [5]. The relative ability of a paramagnetic Gd(III) complex to act as an MRI contrast agent is expressed by its relaxivity, which measures the relaxation enhancement of water protons in solution containing the paramagnetic agent at 1 mM concentration [6]. Many efforts have been devoted to improving the relaxivity of Gd(III)-based contrast agents. As recognized early, high relaxivities can be achieved for slow-moving systems endowed with long rotational correlation times, fast exchange rates of the coordinated water molecules, and suitably long electronic relaxation rates of the unpaired electrons on the metal ion [1, 4].

On this basis several macromolecular systems have been designed in which the Gd(III) complexes are either covalently or noncovalently bound to high molecular weight substrates. Many supramolecular systems have been developed, such as dendrimers [7], polymers [8], proteins [9], water–gadofullerenes [10], and supramolecular amphiphilic aggregates such as micelles [11] and liposomes [12].

Among these carriers, micelles and liposomes, because of their easily controlled properties and good pharmacological characteristics, such as long blood retention, high tissue perfusion or excretion, are very promising candidates as contrast agents. The molecular targeting of supramolecular aggregates containing contrast agents might be accomplished by conjugating active recognition moieties, such as peptides [13] or antibodies [14], to their surface. For example, these bioactive markers could deliver the aggregates to membrane receptors overexpressed by cancerous cells [15].

We have recently developed mixed micellar aggregates containing a large number of gadolinium complexes and several units of a bioactive peptide, coupling together in the same contrast agent the high relaxivity due to the large number of paramagnetic complexes and the target specificity of the bioactive peptide [11, 16–18]. The CCK8 peptide (amino acid sequence Asp-Tyr-Met-Gly-Trp-Met-Asp-Phe-amide) is the C-terminal end of the peptide hormone cholecystokinin. This bioactive peptide should be able to deliver the aggregates on the cholecystokinin receptors CCK_A-R and/or CCK_B-R [19]. In this paper we describe new pure and mixed supramolecular structures in which both the amphiphilic monomers are represented by "gemini" surfactants. In general, as is well known, gemini surfactants are formed by the covalent linking of two "conventional" surfactants via a spacer [20, 21]. These surfactants have interesting features, such as low critical micellar concentration (cmc) values, which drastically reduce cytolytic action on the cell membrane. By manipulating the molecular architecture and the solution conditions, one can obtain a variety of supramolecular aggregates, such as vesicles and micelles. In the last few

years, Camilleri et al. proposed a novel class of peptide-based cationic gemini surfactants as nonviral gene-transfer vectors. These gemini surfactants include C12 saturated hydrocarbon "tails" and a short peptide "head group" with one or more basic amino acid residues. They were synthesized by starting from the reaction of L-cysteine with dibromoethane to form the bisthioether [22, 23] or by using a spermine molecule as a linker [24]. We have developed a new synthetic procedure in the solid phase to easily obtain gemini-based peptide surfactants by introducing a cysteine residue in the peptide sequence. This strategy allows disulfur-bridge formation under mild oxidative conditions, reducing the number of purification steps. The new strategy was applied in the work reported here for the achievement of two gemini surfactants: one containing the bioactive sequence of the cholecystokinin peptide CCK8, [C18CysL5CCK8]$_2$, and the other one containing the chelating agent DTPAGlu or its gadolinium complex, DTPAGlu(Gd), [C18CysDTPAGlu(Gd)]$_2$ (see Fig. 1). We also report on the structural characterization and on the relaxivity behavior of supramolecular aggregates obtained by coassembling the two synthetic gemini surfactants at 70:30 molar ratio between the chelating monomer or its corresponding gadolinium complex and peptide monomer. Moreover, on the basis of recent reports in the literature which suggest conformational changes of the peptide upon temperature increase [25, 26] and to highlight the structural behavior of these aggregates as function of temperature [27, 28], we also performed structural investigations over a wide temperature range. These supramolecular aggregates represent the first example of peptide-containing gemini surfactants as potential target-selective contrast agents in MRI.

Results and discussion

Both gemini surfactants were synthesized by solid-phase methods using Rink amide 4-methylbenzhydrylamine (MBHA) resin as a polymeric support and 9-fluorenyl-methoxycarbonyl(Fmoc)/*t*-Bu chemistry according to standard solid phase peptide synthesis protocols [29]. After the cleavage from the resin, the crude monotailed products were dissolved in an ammonium hydrogen carbonate solution (pH 8.0–8.5) and stirred at room temperature for 24 h [see Fig. S1 for liquid chromatography (LC)–mass spectrometry (MS) data of crude products). The oxidation reactions were followed by using the colorimetric Ellmann test [30]. In Fig. 2 the ^1H NMR spectrum of C18Cys-DTPAGlu monomer in dimethyl-d_6 sulfoxide (DMSO-d_6) before its oxidation to the corresponding gemini surfactant is shown. The NMR spectrum confirms the high purity of the product, allowing a good yield of the oxidized gemini
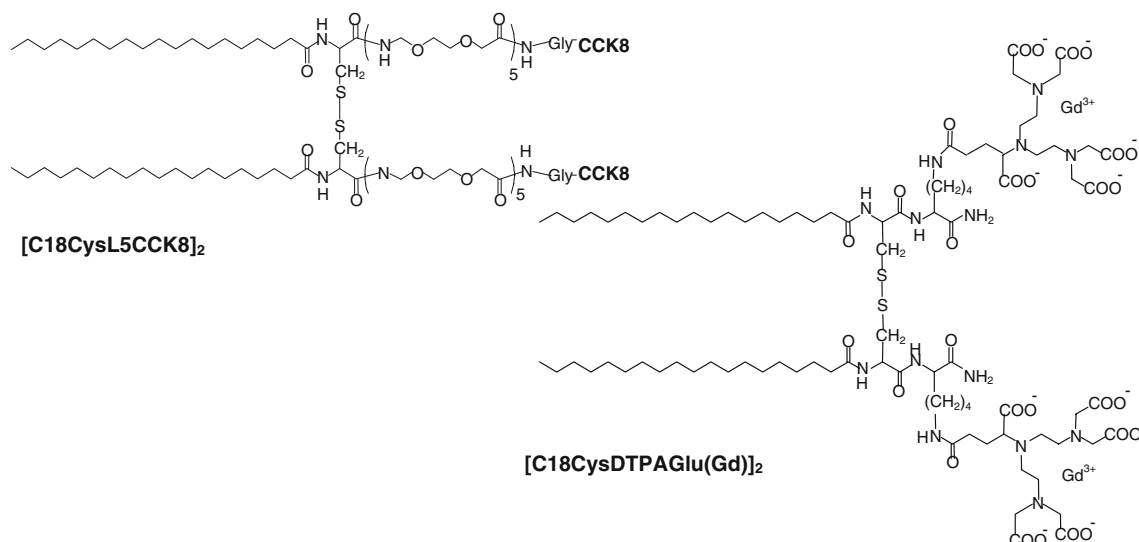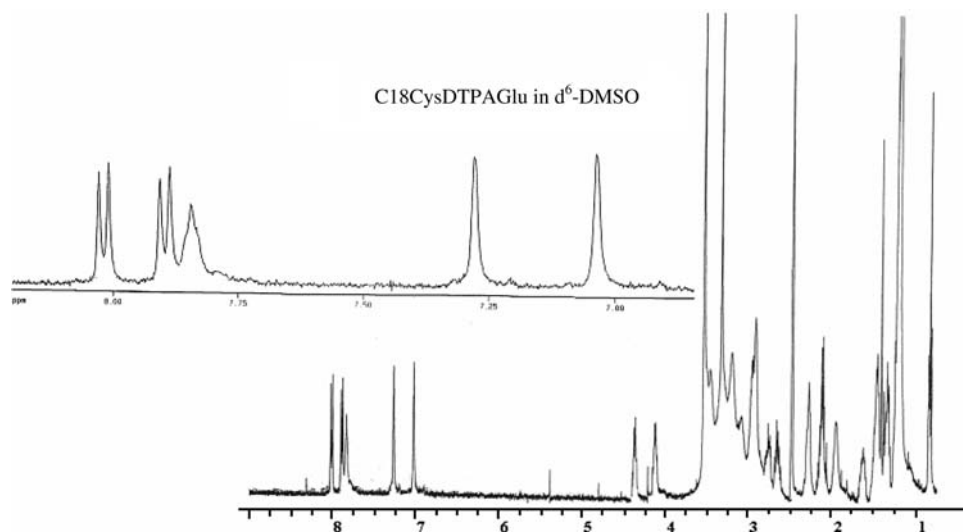
Fig. 1 [C18CysDTPAGlu(Gd)]₂ and [C18CysL5CCK8]₂ gemini amphiphilic monomers, obtained by connecting two identical moieties by a disulfide bond

Fig. 2 ¹H NMR spectrum of C18CysDTPAGlu in dimethyl-d_6 sulfoxide

surfactant. As is clearly visible in the enlarged low-field region, the spectrum presents a broad signal (7.80 δ) corresponding to the $^{\varepsilon}$NH-Lys proton, and two doublets related to $^{\alpha}$NH amide protons of the Cys–Lys fragment. These signals (8.05 and 7.90 δ) are shifted at high field compared with the NH signal in random-coil peptide chains (8.40–8.30 δ). The [C18CysL5CCK8]₂ gemini surfactant was purified by preparative reversed-phase high-performance LC (HPLC) to a final HPLC purity of 90% and was isolated in 25% yield in lyophilized form. Analytical LC-MS data confirm the identity of the compound and its high purity. The gadolinium complex of [C18CysDTPAGlu]₂ was prepared by adding 2 equiv of GdCl₃ to a [C18Cys-DTPAGlu]₂ ligand solution at neutral pH and room temperature. To avoid the relaxivity contribution of free gadolinium ion, the excess was removed by filtering the

complex solution left at pH 10 for 24 h with a 0.2-μm syringe filter, as already reported for other chelating amphiphilic monomers [11]. The xylenol orange UV-spectrophotometric method was used to check for the absence of free Gd(III) ions [31]. Self-assembling and mixed supramolecular aggregates were obtained by simply dissolving [C18CysDTPAGlu]₂ (or its corresponding gadolinium complex) and [C18CysL5CCK8]₂ gemini surfactants in phosphate buffer at pH 7.4.

Structural characterization

Fluorescence measurements

Cmc values of [C18CysDTPAGlu]₂–H₂O, [C18CysDTP-AGlu(Gd)]₂–H₂O, and [C18CysL5CCK8]₂–H₂O binary

systems and of [C18CysDTPAGlu]$_2$–[C18CysL5CCK8]$_2$–H$_2$O and [C18CysDTPAGlu(Gd)]$_2$–[C18CysL5CCK8]$_2$–H$_2$O ternary systems were determined by steady-state fluorescence spectroscopy by using, in separate experiments, two different probes: 8-anilinonaphthalene-1-sulfonate (ANS) and pyrene. The cmc measurements by two independent experiments allow minimization of the uncertainty in the calculated values. ANS and pyrene are both fluorescent probes that are poorly soluble in aqueous solution that change their emission spectrum depending on the polarity of the environment (hydrophobic or hydrophilic). The ANS fluorophore fluoresces at 480 nm only in a hydrophobic environment such as the inner micelle core [32]; thus, when the fluorescence intensity at 480 nm is plotted as a function of the amphiphile concentration, the breakpoint indicates the cmc value (see Fig. 3a, c, Table 1). In contrast, the pyrene molecule shows a more complex emission spectrum composed of five emission peaks (373, 379, 383, 389, and 393 nm). These peaks are affected by the polarity of the surrounding environment of the probe molecules. Specifically, it is considered that the I_1/I_3 ratio of pyrene fluorescence is an index of the polarity of its environment. The values in hydrophobic solvents vary in the range 0.57–0.61, while in polar solvents the range is 1.25–2.00. In a micellar medium the observed values can be explained in terms of penetration of water into micelles and of the type of surfactant head group [33, 34].

As shown in Fig. 3b and d, the ratio between the intensities of the first (I_1) and the third (I_3) vibration bands of the pyrene emission spectrum remains constant (approximately 1.4–1.5) at monomer concentrations $c \leq 10^{-6}$ mol kg^{-1}, thus indicating the absence of micellar aggregates. At higher concentrations ($c > 10^{-6}$ mol kg^{-1}) I_1/I_3 decreases, thus indicating surfactant aggregation and pyrene migration from the aqueous environment into the hydrophobic core (or at the core–corona interface). Even though it has been reported that the polarity of the outer layer of the micelles could influence the pyrene emission [35], the cmc values obtained by using ANS and pyrene methods are in good agreement and indicate that all monomers in aqueous solution aggregate above a molal concentration in the

Fig. 3 a, c Fluorescence intensity of the 8-anilinonaphthalene-1-sulfonate fluorophore at 480 nm and b, d I_1/I_3 ratio of the pyrene vibration band versus surfactant concentration: [C18CysDTPAGlu]$_2$–H$_2$O (squares); [C18CysL5CCK8]$_2$–H$_2$O (open circles); [C18CysDTPAGlu(Gd)]$_2$–H$_2$O (filled circles); [C18CysDTPAGlu]$_2$–[C18CysL5CCK8]$_2$–H$_2$O (open triangles); [C18CysDTPAGlu(Gd)]$_2$–[C18CysL5CCK8]$_2$–H$_2$O (filled triangles). The data were multiplied by a scale factor for better comparison
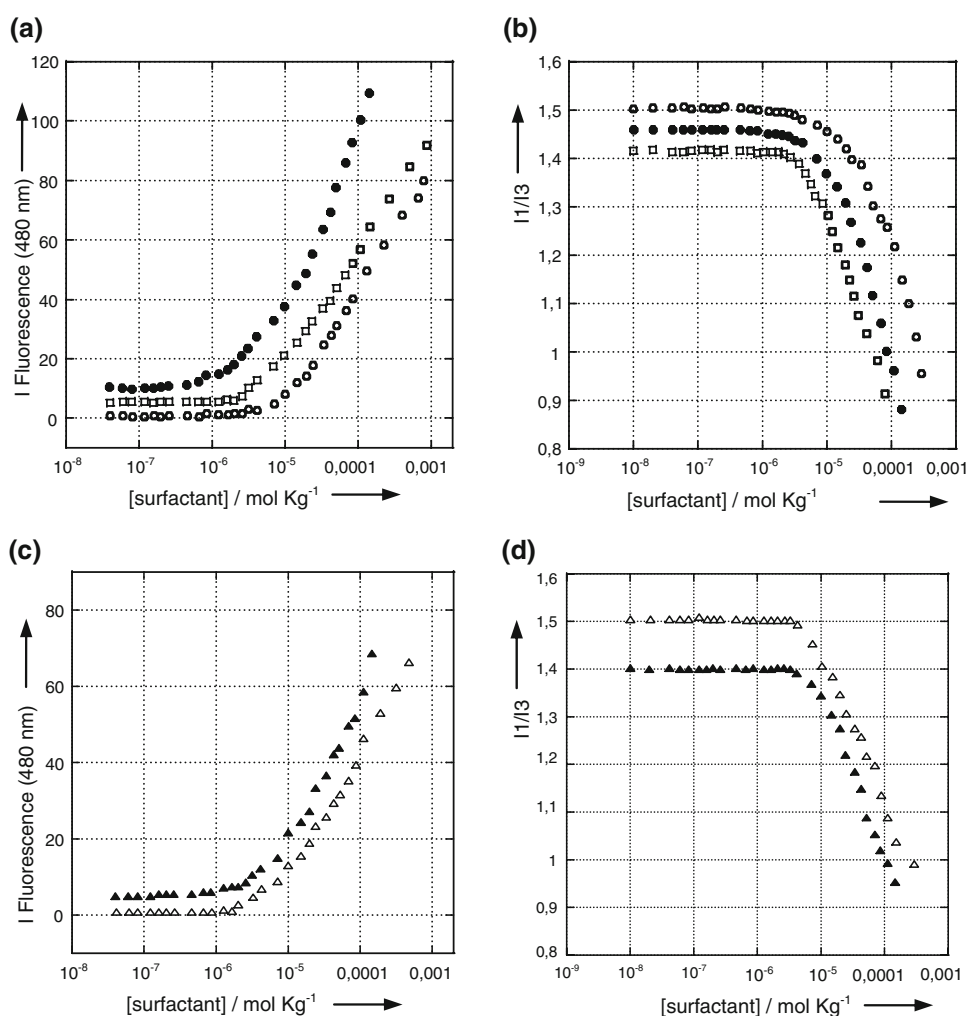
Table 1 Critical micellar concentration (*cmc*) values of supramolecular aggregates determined by steady-state fluorescence spectroscopy using 8-anilinonaphthalene-1-sulfonate (*ANS*) and pyrene as probes

System	ANS cmc (mol kg^{-1})	Pyrene cmc (mol kg^{-1})
[C18CysDTPAGlu]$_2$–H$_2$O	4.3×10^{-6}	4.8×10^{-6}
[C18CysDTPAGlu(Gd)]$_2$–H$_2$O	1.0×10^{-5}	1.5×10^{-5}
[C18CysL5CCK8]$_2$–H$_2$O	5.5×10^{-6}	6.5×10^{-6}
[C18CysDTPAGlu]$_2$–[C18CysL5CCK8]$_2$–H$_2$O	5.3×10^{-5}	5.6×10^{-5}
[C18CysDTPAGlu(Gd)]$_2$–[C18CysL5CCK8]$_2$–H$_2$O	8.0×10^{-6}	8.0×10^{-6}

See Fig. 1 for the molecular structures

5×10^{-6}–5×10^{-5} mol kg^{-1} range (see Table 1). These values are only slightly lower than the cmc values for the aggregates previously obtained by self-assembly of mono-tailed monomers (5×10^{-5} mol kg^{-1}) [11, 36]. This experimental result is apparently in disagreement with the well-known gemini surfactant properties, consisting of the ability of gemini surfactants to aggregate at cmc values lower than those of the monotailed monomers. In more detail, [C18CysDTPAGlu]$_2$ has a cmc value of approximately 4.6×10^{-6} mol kg^{-1}, while the corresponding monotailed monomer C18DTPAGlu has a cmc value of 5×10^{-5} mol kg^{-1}. These results can be explained taking into account the high electrostatic repulsion between the negative charges of the [C18CysDTPAGlu]$_2$ head groups. This monomer contains two DTPAGlu chelating agents in the same molecule, where each DTPAGlu moiety has five negative charges (COO$^-$) at physiological pH, or two negative charges after gadolinium complexation. The cmc values are slightly higher than those found for double-tailed amphiphiles bearing only one charged DTPAGlu head group [16]. Hence, in the gemini compound two different effects are present : the higher tendency to aggregate with respect to the monotailed monomers, and the higher electrostatic repulsion between the head groups due to the negative charges of DTPAGlu moieties. The combination of these two effects produces (1) a slight stabilization of the gemini compound with a cmc value only 1 order of magnitude lower than for the monotailed monomer and (2) a slight loss in stability with respect to (C18)$_2$DTPAGlu. The cmc value (approximately 6×10^{-6} mol kg^{-1}) found for [C18CysL5CCK8]$_2$ monomer, in which there are no repulsion effects, is in agreement with the low expected values for gemini surfactants. In fact, the corresponding monotailed monomer (C18L5CCK8) did not show any tendency to aggregate under the same experimental conditions [36]. Moreover, fluorescence spectroscopy was used to confirm the presence of the bioactive peptide that is well exposed on the aggregate external surface: fluorescence at

approximately 360 nm of the tryptophan indole moiety (Fig. S2) is indicative of the presence of a tryptophan residue in a polar aqueous solvent, suggesting the presence of the entire CCK8 peptide in the micellar external environment.

Circular dichroism

The secondary peptide structures in pure aggregates formed by [C18CysL5CCK8]$_2$ and in [C18CysDTPAGlu]$_2$–[C18CysL5CCK8]$_2$ mixed aggregates [and the corresponding system in which the DTPAGlu chelating agent complexes the Gd(III) ion] were evaluated by circular dichroism (CD) spectroscopy. As was expected for short peptide sequences [37], and as previously reported [38, 39], the CCK8 octapeptide moiety does not undergo any folding process in water solution. On the other hand, in micellar aggregates obtained by self-assembly of (C18)$_2$L5CCK8, the peptide shows a classic β-sheet fold [40]. This result suggests that the hydrogen bonds among amino acids, well exposed on the external surface of the aggregates, promote intermolecular sheet-like structures that are stabilized by interactions between the alkyl chains. In the present case, according to the previous results, the CD spectrum of [C18CysL5CCK8]$_2$ reveals the characteristic shape of a β-sheet-type structure (Fig. 4). Upon heating the solution, the intensity of the CD spectra of the β-sheet structure signals (222 nm) decreases linearly, suggesting the breaking up of the interactions between peptides that are near each other. By plotting the intensity of the CD spectra at 222 nm as a function of temperature, one obtains a sigmoid curve composed of three temperature ranges: in the first one (from 10 °C to approximately 20 °C) the CD signal remains constant; in the second one (from approximately 20 °C to approximately 60 °C) there is a progressive decrease of the CD signal; and in the last one (from approximately 60 °C to 80 °C) the signal intensity remains constant. The maximum in the first derivative of the sigmoid curve indicates the transition temperature ($T_t \sim 45$ °C) at which the peptide structure changes from a β-sheet to a random-coil structure. The random-coil structure observed at 80 °C persists when the samples are cooled down. The peptide β-sheet conformation seems to be again obtained only below 20 °C, indicating a hysteresis phenomenon at the cooling rate used (1 °C min^{-1}). Similar structural behavior of the CCK8 peptide is observed in the case of the two mixed aggregates [C18CysDTPAGlu]$_2$–[C18CysL5CCK8]$_2$ and [C18CysDTPAGlu(Gd)]$_2$–[C18CysL5CCK8]$_2$, with T_t values in the same range (Fig. 5), and the presence of the hysteresis phenomenon. This result indicates that in mixed micelles, in which the two monomers [C18CysDTPAGlu]$_2$ and [C18CysL5CCK8]$_2$ are combined in 70:30 molar ratio, CCK8 molecules, notwithstanding their dilution in
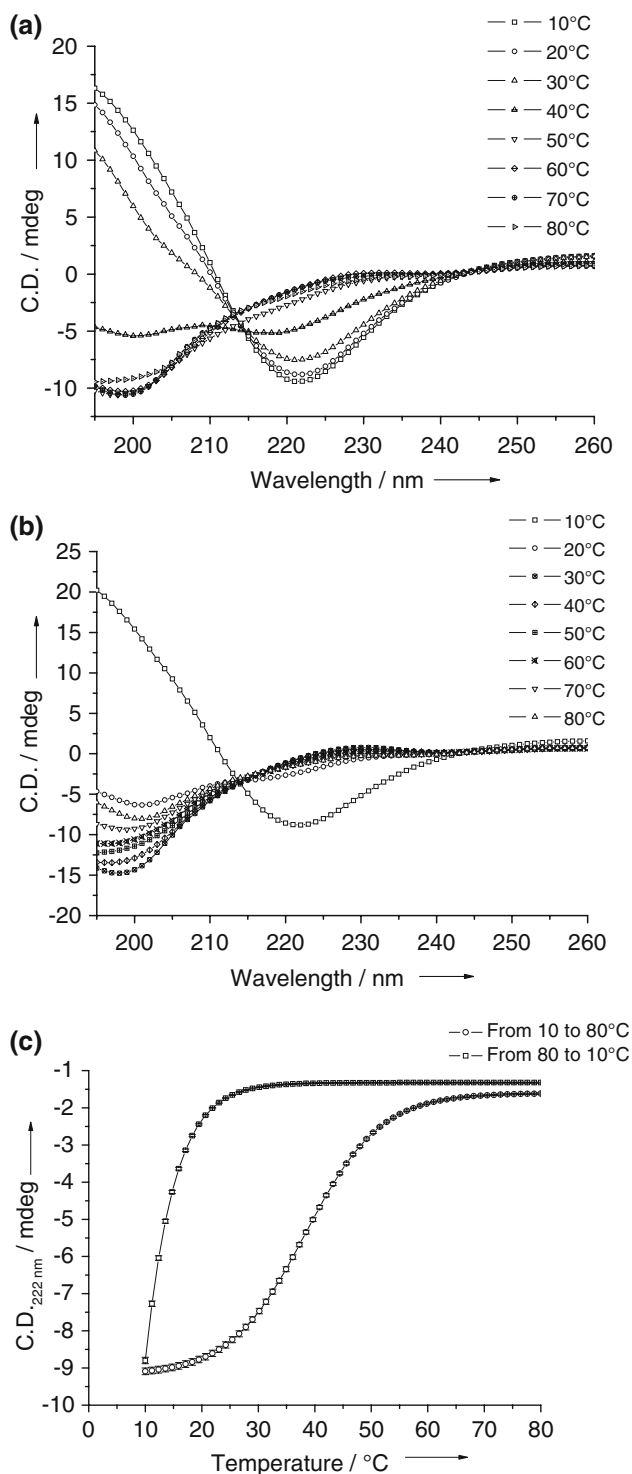
Fig. 5 Circular dichroism spectra of the [C18CysDTPAGlu(Gd)]₂–[C18CysL5CCK8]₂–H₂O ternary system (70:30 molar ratio, pH 7.4, 1×10^{-4} M concentration of the peptide-containing gemini surfactant) at different temperatures. The heating curve of the circular dichroism signal at 222 nm (from 10 to 80 °C) is shown in the *inset*

Small-angle neutron scattering

Small-angle neutron scattering (SANS) provides a direct probe of aggregate structure in dilute solutions. Figure 6 show the scattering cross sections collected for the [C18CysDTPAGlu(Gd)]₂ (1.40 mmol kg⁻¹)–[C18CysL5-CCK8]₂ (0.60 mmol kg⁻¹)–D₂O ternary system. The scattering cross sections for the [C18CysL5CCK8]₂ binary system and for the corresponding ternary systems containing [C18CysDTPAGlu]₂ are reported in Figs. S3 and S4. Figure 6a shows cross sections measured with temperature increasing, at 10, 40, 60, and 80 °C, and Fig. 6b shows cross sections measured with temperature decreasing, at 50, 20, and 10 °C. Inspection of the data shows some characteristic behavior for all the systems. The absence of a peak or depression of the signal at lower q suggests minimal, if any, intermicellar $S(q)$ interaction, as would be expected at these low concentrations in a 0.1 M buffer solution.

At 10 and 40 °C in Fig. 6a, the intensity for the initially prepared solutions scales with a $d\Sigma/d\Omega \propto q^{-1}$ power law characteristic of elongated structures (i.e., rod-like micelles). Owing to the lack of the Guinier regime for such temperatures, it is possible only to estimate that the length l of the cylinders should be greater than $2\pi/q_{min}$, where q_{min} is the smallest q value explored with the SANS measurements. The length of the rods is thus likely to be more than 700 Å. The radius of the cylindrical structures can be found from the axial Guinier equation for long, thin, rigid rods [41]:

$$\ln\left(q\frac{d\Sigma}{d\Omega}\right) = \ln\left(\phi(1-\phi)\pi R^2 \Delta^2 \rho\right) - \frac{q^2 R^2}{4}. \qquad (1)$$

By fitting of Eq. 1 in the q range where $q \ll \pi/R$, cylindrical radii R of 19–24 Å were obtained, as reported in

Fig. 4 Circular dichroism spectra of 1×10^{-4} M [C18CysL5-CCK8]₂ aggregate solution at pH 7.4: **a** aggregate solution heated from 10 to 80 °C; **b** aggregate solution cooled from 80 to 10 °C; **c** heating and cooling curves of the circular dichroism signal at 222 nm (from 10 to 80 °C and from 80 to 10 °C)

[C18CysDTPAGlu]₂ aggregates, are still close enough to each other to maintain hydrogen bonds among peptide chains.
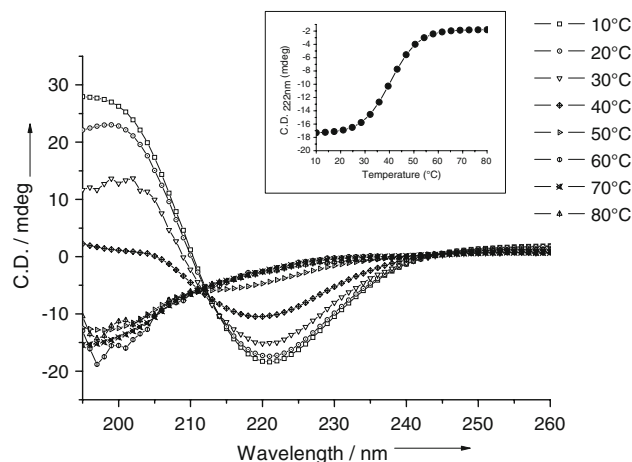
Fig. 6 Scattering cross sections measured on heating (**a**) and cooling (**b**) the [C18CysDTPAGlu(Gd)]$_2$ (1.40 mmol kg^{-1})–[C18CysL5CCK8]$_2$ (0.60 mmol kg^{-1})–D$_2$O system, at the temperatures reported. To make the data more readable, cross sections were multiplied by a scale factor, as indicated
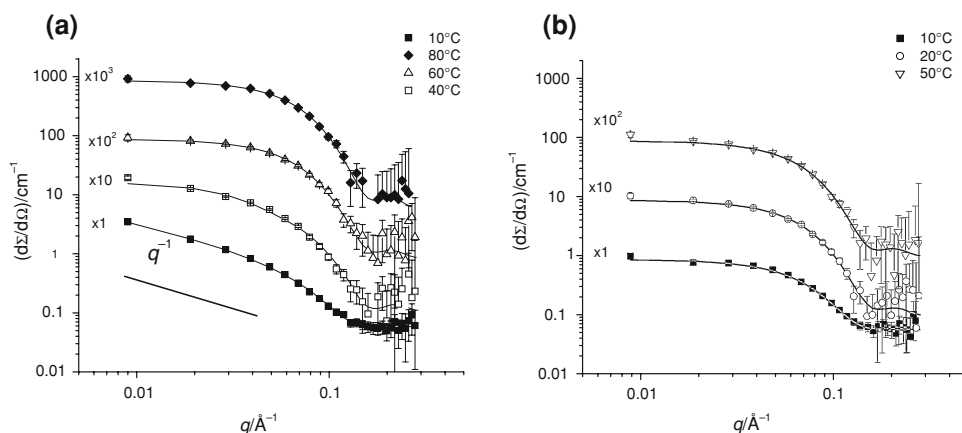
Table 2. It is worth noting that the flat background was taken into account for correct evaluation of the radius. Upon increasing the temperature above 40 °C, the aggregates change shape and the data suggest a form factor typical of ellipsoidal aggregates (see Figs. 6b, S3, S4). This behavior holds up to the highest temperature investigated (80 °C) and persists even when the samples are cooled down: the structural features seem to be preserved even if the initial temperature (10 °C) is again reached. Thus, we are in the presence of a hysteresis phenomenon. Scattering cross sections were modeled for a collection of monodisperse ellipsoidal micelles with an

aggregation number N_{agg} of surfactant molecules with volume v. When significant interactions among the aggregates can be excluded, the scattering cross sections dΣ/dΩ can be expressed as [42]

$$\frac{d\Sigma}{d\Omega} = n_p P(q) + \left(\frac{d\Sigma}{d\Omega}\right)_{incoh}, \qquad (2)$$

where n_p is the number density of scattering bodies, $P(q)$ is the form factor of the bodies, and $(d\Sigma/d\Omega)_{incoh}$ is the incoherent scattering cross section. By modeling the micelles as uniform ellipsoids with semiaxes a, $b = c$, one can write the function $P(q)$ as

Table 2 Structural parameters obtained from fitting to small angle neutron scattering data at different temperatures

	10 °C	40 °C	50 °C	60 °C	80 °C	50 °C	20 °C	10 °C
[C18CysL5CCK8]$_2$ (1.00 mmol kg^{-1})–D$_2$O								
N_{agg}	–^{a}	–^{a}	–	16 ± 1	15 ± 1	14 ± 1	14 ± 1	13 ± 1
R (Å)	21 ± 1	22 ± 1	–					
a (Å)			–	43 ± 2	42 ± 2	41 ± 2	41 ± 2	40 ± 2
$b = c$ (Å)			–	25 ± 1	25 ± 1	24 ± 1	24 ± 1	24 ± 1
[C18CysDTPAGlu(Gd)]$_2$ (1.40 mmol kg^{-1})–[C18CysL5CCK8]$_2$ (0.60 mmol kg^{-1})–D$_2$O								
N_{agg}	–^{a}	–^{a}	26 ± 1	22 ± 1	23 ± 1	22 ± 1	21 ± 1	21 ± 1
R (Å)	24 ± 1	23 ± 1						
a (Å)			57 ± 2	43 ± 2	46 ± 2	44 ± 2	44 ± 2	42 ± 2
$b = c$ (Å)			24 ± 1	25 ± 1	25 ± 1	25 ± 1	25 ± 1	25 ± 1
[C18CysDTPAGlu]$_2$ (1.40 mmol kg^{-1})–[C18CysL5CCK8]$_2$ (0.60 mmol kg^{-1})–D$_2$O								
N_{agg}	–^{a}	–^{a}	26 ± 1	25 ± 2	21 ± 1	21 ± 1	22 ± 1	23 ± 1
R (Å)	23 ± 1	19 ± 1						
a (Å)			57 ± 2	46 ± 2	44 ± 2	47 ± 2	46 ± 2	44 ± 2
$b = c$ (Å)			24 ± 1	24 ± 1	25 ± 1	24 ± 1	25 ± 1	26 ± 1

The equations used for the fitting are in the text. The radius (R) of cylindrical aggregates obtained at lower temperature is reported in the first two columns; the length of the semiaxis (a, $b = c$) of ellipsoidal micelles found at higher temperature and by cooling them to 10 °C is reported in the other columns

^{a} The aggregation number, N_{agg}, is not measurable in the case of cylindrical aggregates

$$P(q) = (\Delta\rho)^2 V^2 \int_0^1 F(q,\mu)^2 d\mu, \qquad (3)$$

where $F(q,\mu)$ is the angle-dependent form factor for ellipsoidal micelles

$$F(q,\mu) = \frac{3j_1(u)}{u}, \qquad (4)$$

with

$$u = q\sqrt{\mu^2 a^2 + (1-\mu^2)b^2}, \qquad (5)$$

where j_1 is the spherical Bessel function of first order, $V = 4/3\pi ab^2 = vN_{agg}$ is the micellar volume, and $\Delta\rho$ is the contrast existing between the micelles and the solvent. By using Eqs. 2, 3, 4, and 5, we obtained structural information on the aggregates present in the system and this is reported in Table 2.

Inspection of Table 2 reveals that micellar aggregates have elongated shapes with a cylindrical structure at lower temperatures and ellipsoidal shapes (with an axes ratio of approximately 2) at higher temperatures. The similar values observed for the radius of the cylindrical structures and for the minor semiaxis of the ellipsoidal structures suggest that the increase of the temperature leads to progressive shortening of the cylindrical structures to ellipsoidal micelles. Furthermore, the cooling of the systems again to 10 °C, once they have reached the maximum temperature investigated (80 °C), does not produce a significant change in the size and shape of the micelles.

Relaxivity measurements

The measured relaxivity value (r_{1p}) is defined, according to Eq. 6, as the paramagnetic contribution to the measured proton longitudinal relaxation rate (R_{1obs}) of a solution containing 1.0 mM concentration of the paramagnetic solute:

$$R_{1obs} = [Gd]r_{1p} + R_{1W}, \qquad (6)$$

where R_{1w} is the diamagnetic contribution of pure water (0.38 s^{-1}). Relaxivity values at 20 MHz and 25 °C

(Table 3) were determined by mineralizing a 100-μl sample with 100 μl of 37% HCl at 120 °C overnight to determine the exact concentration of Gd(III) present in the solutions.

This mineralization process leads to a complete destruction of the gadolinium complex with the consequent release of free Gd(III) aquaion in the acidic solution. From the value of the observed relaxation rate (R_{1obs}) of this acidic solution, and knowing the relaxivity (r_{1p}) of Gd(III) aquaion in acidic conditions (13.5 mM^{-1} s^{-1} at 20 MHz and 25 °C—GdCl$_3$ solutions whose concentrations were measured by inductively coupled plasma MS were used as standards, accuracy ±0.1%) and the diamagnetic contribution (R_{1w}) in acidic conditions (0.5 mM^{-1} s^{-1}), we calculated the exact Gd(III) concentration using Eq. 6. Then, knowing the GdL concentration (opportunely corrected for the 1:1 acidic dilution) and measuring R_{1obs} of the aggregate-containing sample solutions, we calculated the relaxivity values of the two systems considered using again Eq. 6. The relaxivity measurements were performed on samples at a concentration much higher than the cmc: under these conditions, the contribution of monomeric species is negligible, and only aggregates are responsible for the measured relaxivity values. All the relaxometric characterization was conducted at 25 °C, that is, in the temperature conditions for which micelles have a rod-like cylindrical shape. The relaxivity values determined at 25 °C and 20 MHz are 18.4 and 21.5 mM^{-1} s^{-1} for pure and mixed micelles respectively. These values are in accordance with those of other similar gadolinium-containing micellar systems, as almost all the $q = 1$ (one inner-sphere water molecule) gadolinium-based micelles have relaxivity values in the range 18–23 mM^{-1} s^{-1} (20 MHz, 25 °C) [43–45]. To reach high relaxivity values, a very important parameter to account for is the exchange lifetime of the coordinated water molecule (τ_M) of a Gd(III) complex. The analysis of the temperature dependence of the transverse relaxation rate of the metal-bound ^{17}O water resonance may be considered the method of choice for the determination of τ_M values [46, 47]. The τ_M value determined for the [C18CysDTPA-Glu(Gd)]$_2$ self-assembling aggregate at 25 °C and neutral pH was 152 ns. In the case of the [C18CysDTPAGlu(Gd)]$_2$–

Table 3 Principal relaxometric parameters measured at pH 7.4, 25 °C, and 20 MHz, calculated from fitting the nuclear magnetic relaxation dispersion (τ_R, Δ^2, τ_V) and ^{17}O NMR (τ_M) data as described in the text

System	r_{1p} (mM^{-1} s^{-1})	τ_M (ns)	τ_R (ns)			Δ^2 ($\times 10^{18}$ s^{-2})	τ_V (ps)
			τ_1	S	τ_g		
[C18CysDTPAGlu(Gd)]$_2$–H$_2$O	18.4	152	0.190	0.49	3.20	7.65	57.3
[C18CysDTPAGlu(Gd)]$_2$–[C18CysL5CCK8]$_2$–H$_2$O	21.5	152[a]	0.533	0.41	3.20	9.09	50.0

[a] The exchange lifetime of the peptide-containing system was assumed to be similar to that of the corresponding system not containing the peptide
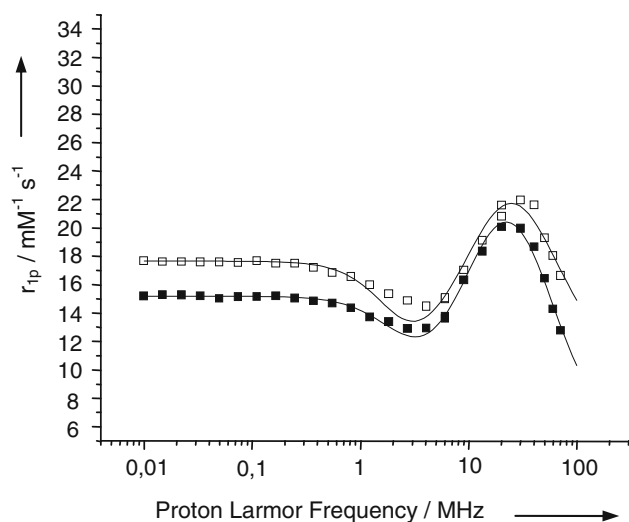
Fig. 7 Nuclear magnetic resonance dispersion profiles of [C18Cys-DTPAGlu(Gd)]$_2$ (*filled squares*) and [C18CysDTPAGlu(Gd)]$_2$–[C18CysL5CCK8]$_2$ (*open squares*) obtained at pH 7.4 and 25 °C, normalized to 1 mM concentration of Gd(III) ion. The *curves* through the data points were calculated with the parameters reported in Table 3

[C18CysL5CCK8]$_2$ mixed aggregate the τ_M value was assumed to be the same as that of the pure [C18Cys-DTPAGlu(Gd)]$_2$. From a quantitative analysis of the nuclear magnetic relaxation dispersion (NMRD) profiles it is possible to determine the reorientational correlation time (τ_R), which is related to the size of the system investigated. The NMRD profiles of [C18CysDTPAGlu(Gd)]$_2$ and [C18Cys-DTPAGlu(Gd)]$_2$–[C18CysL5CCK8]$_2$ at 25 °C are reported in Fig. 7. For the micellar systems, the data were analyzed using the Solomon–Bloembergen–Morgan model modified according to the Lipari–Szabo approach [48, 49]. This approach distinguishes between two independent motions: a rapid local motion governed by a correlation time defined as τ_l and a slower global motion with a correlation time defined as τ_g. Data resulting from the fitting of the NMRD profiles are reported in Table 3. The analysis of experimental data gave the same value for τ_g of the two gadolinium-containing systems, that is, only slightly higher than the values reported for other gadolinium-based micellar systems [46].

The two systems differ substantially in the value of τ_l as it seems that in mixed micelles containing the CCK8 amphiphilic moiety the internal motility of gadolinium-containing units is reduced. Clearly the complexes give rise to a system with a slower molecular tumbling in comparison with isolated gadolinium complexes. Anyway, the resulting relaxivity appears still lower than the expected values as internal motions are faster than the overall tumbling of the micellar system. According to the recent theory of Nicolle et al. [50], a relaxivity value lower than the theoretic one can be also ascribed to the interactions between nearby paramagnetic centers in micellar systems

which increase the transverse electronic relaxation of the electron spins of Gd(III) and, therefore, reduce the attainable water proton relaxivity. In this case, the proximity between Gd(III) centers is not only given by micellar assembly but also by the dimeric nature of the amphiphilic units.

Conclusion

The new gemini surfactants [C18CysL5CCK8]$_2$ and [C18CysDTPAGlu]$_2$ or its gadolinium complex [C18Cys-DTPAGlu(Gd)]$_2$ were prepared following a new efficient synthetic strategy. According to this strategy, amphiphilic monomers are synthesized using solid-phase methods, and after purification they are linked together through a disulfide bond between two cysteine residues, to give the corresponding gemini surfactants.

Gadolinium-based paramagnetic supramolecular aggregates derivatized with bioactive peptides, acting as selective contrast agents, have already been developed, by us and others, using different synthetic approaches [51, 52]. They are capable of visualizing neovascularization and angiogenic processes targeting $\alpha_v\beta_3$ integrins or tumor proliferation and metastasis, targeting cellular receptors overexpressed by cancer cells. The choice of synthetic strategy depends on whether coupling is performed before or after assembly of the supramolecular aggregate. The obvious goal of each approach is to achieve high coupling efficiency, but with the ligand retaining full binding affinity for its target receptor. The coupling of a ligand after the aggregate has been assembled involves the introduction of suitable activated functional groups onto the terminus of one of the aggregate components. Labeling procedures, based on the use of amphiphilic peptides that assemble together with amphiphilic gadolinium complexes in the peptide-labeled supramolecular aggregates, are very effective and have been used by us to have CCK8-labeled paramagnetic micelles and liposomes [11, 16–18]. The supramolecular aggregates reported here were structurally identified as cylindrical or ellipsoidal micelles. The shape and size of the micelles are influenced by the temperature: at lower temperatures micellar aggregates have elongated shapes with a cylindrical structure, while at higher temperatures ellipsoidal shapes are found. It seems that the increase of the temperature leads to progressive shortening of the cylindrical structures to ellipsoidal micelles. Likewise, the surface-exposed CCK8 peptide changes its conformation on increasing the temperature, going from a β-sheet to a random-coil structure. Even if there is any evidence that the two phenomena are related, the similarity of the transition temperatures of the two processes as well as the amplitude of the hysteresis indicate a possible

cooperation between the aggregate structure transition and the peptide conformation variation. The aggregates obtained by coaggregation of the two gemini-surfactant-based amphiphilic compounds, [C18CysDTPAGlu(Gd)]$_2$ and [C18CysL5CCK8]$_2$ in 70:30 molar ratio, represent the first example of peptide-containing gemini surfactants as potential target-selective contrast agents in MRI. The high relaxivity value, 21.5 mM^{-1} s^{-1}, and the presence of CCK8 bioactive peptide exposed on the external surface of the micellar aggregate make this compound very attractive as an MRI contrast agent for in vivo visualization of tumor cells overexpressing the cholecystokinin receptors [53].

Materials and methods

Materials

Protected N^α-Fmoc-amino acid derivatives, coupling reagents and Rink amide MBHA resin were purchased from Calbiochem-Novabiochem (Laufelfingen, Switzerland). Fmoc-8-amino-3,6-dioxaoctanoic acid (Fmoc-AdOO-OH) was purchased from Neosystem (Strasbourg, France). The DTPAGlu pentaester, *N,N*-bis[2-[bis[2-(1,1-dimethyletoxy)-2-oxoethyl]-amino]ethyl]-L-glutamic acid 1-(1,1-dimethylethyl)ester, was prepared according to the experimental procedure reported in the literature [54]. All other chemicals were commercially available from Sigma-Aldrich, Fluka (Buchs, Switzerland), or LabScan (Stillorgan, Dublin, Ireland) and were used as received unless stated otherwise. All solutions were prepared by weight using doubly distilled water. Samples to be measured by SANS techniques were prepared using D$_2$O (Sigma-Aldrich, purity better than 99.8%). The pH of all solutions was kept constant at 7.4. Preparative HPLCs were carried out using an LC8 Shimadzu HPLC system (Shimadzu, Kyoto, Japan) equipped with a UV lambda-Max model 481 detector using a Phenomenex (Torrance, CA, USA) C4 column (300 Å, 250 mm × 21.20 mm, 5 μm) eluted with H$_2$O/0.1% trifluoroacetic acid (TFA) (solvent A) and CH$_3$CN/0.1% TFA (solvent B) from 20 to 95% over 25 min at 20 mL min^{-1} flow rate. LC-MS analysis was performed using a Thermo Electron (Waltham, MA, USA) Finnigan system.

[C18CysL5CCK8]$_2$

Peptide synthesis was carried out in the solid phase with a standard Fmoc strategy [29], by using an Applied Biosystems 433A automatic synthesizer. Rink amide MBHA resin (0.78 mmol g^{-1}, 0.5 mmol scale, 0.640 g) was used. The elongation of the G-CCK8 peptide was achieved by

sequential addition of Fmoc-amino acids with ben-zotriazol-1-yl-oxy-tris(pyrrolidinophosphonium) (PyBop)/1-hydroxybenzotriazole (HOBt) and *N,N*-diisopropylethylamine (DIPEA) (1:1:2) as coupling reagents, in dimethylformamide (DMF) in preactivation mode. The mixture was stirred for 1 h and after filtration the corresponding colorimetric test (Kaiser test) indicated the completion of the coupling. All couplings were performed twice for 1 h, by using an excess of 4 equiv for the single amino acid derivative. Fmoc deprotections were obtained using a 30% solution of piperidine in DMF. When the peptide synthesis was complete, the Fmoc N-terminal protecting group was removed and the five residues of Fmoc-AdOO-OH were condensed, step by step, according to the single coupling procedure by using an excess of 2 equiv. Then, the resin was washed and the terminal Fmoc protection was removed. A 1.171-g (2.0-mmol) amount of FmocCys(triphenylmethyl)-OH was coupled on the resin under stirring. The solution was filtered, the resin washed with three portions of DMF, and the Fmoc protecting group of the cysteine residue removed. To obtain the lipophylic monomer, 0.596 g (2.0 mmol) of nonaoctanoic acid was coupled on the linker-peptide N-terminus by using 1.040 g (2.0 mmol) of PyBop, 0.270 g (2.0 mmol) of HOBt, and 0.668 mL (4.0 mmol) of DIPEA in 4 mL of a 1:1 mixture of DMF and dichloromethane (DCM). The coupling time was 1 h under stirring at room temperature. For deprotection and cleavage, the fully protected resin was treated with a TFA solution containing triisopropylsylane (TIS) (2.0%) and water (2.5%) as scavengers. The free peptide derivative was precipitated in cold ethyl ether (Et$_2$O) and lyophilized from a H$_2$O/CH$_3$CN solution. The analytic LC-MS analysis confirmed the identity of the product. C$_{18}$H$_{37}$CO-Cys-(AdOO)$_5$-G-CCK8 (C18CysL5CCK8): R_t = 20.65 min; [M + 3H]$^+$/3 = 741 amu (molecular weight 2,228).

The intramolecular disulfur bond between cysteine residues was obtained by reaction of the crude product (0.1 mmol; 223 mg) dissolved in 100 mL of 0.1 M ammonium hydrogen carbonate (pH 8.0–8.5) at room temperature for 24 h. The air-oxidation reaction was monitored by the colorimetric Ellmann test [30]. The identification of the oxidized product was confirmed by LC-MS analysis. The crude compound was purified by reversed-phase HPLC. Fractions were characterized by LC-MS analysis to assess purity and molecular weight. Pure fractions were pooled and lyophilized. The total amount of the oxidized gemini product was 550 mg, corresponding to a final yield of 25%. LC-MS characterization confirmed the identity of the oxidized gemini product. [C$_{18}$H$_{37}$CO-Cys-(AdOO)$_5$-G-CCK8]$_2$; R_t = 26.76 min; [M + 3H]$^+$/3 = 1,485 amu (molecular weight 4,456).

[C18CysDTPAGlu]$_2$

Fmoc-Lys(Mtt)-OH (624.79 mg, 1.00 mmol), where Mtt is (4-methylphenyl)diphenylmethyl, activated by 1 equiv of PyBop and HOBt and 2 equiv of DIPEA in DMF was coupled twice to Rink amide MBHA resin (0.78 mmol/g, 0.250 mmol scale, 0.320 g) by stirring the slurry suspension for 1 h. The solution was filtered and the resin washed with three portions of DMF and three portions of DCM. The Mtt protecting group was removed by treatment with 2.0 mL of a DCM/TIS/TFA (94:5:1) mixture. The treatment was repeated several times until the solution became colorless. The resin was washed with DMF and then the DTPAGlu pentaester chelating agent was linked, through its free carboxyl function, to the α-NH$_2$ of the lysine residue. This coupling step was performed using 2.0 equiv of DTPAGlu pentaester and O-(7-azabenzotriazol-1-yl)-1,1,3,3-tetramethyluronium, and 4 equiv of DIPEA in DMF as the solvent. The coupling time, compared with that for the classic solid phase peptide synthesis protocol, was increased up to 2 h and the reaction was tested for completion by the Kaiser test. After removal of the Fmoc protecting group by 30% piperidine in DMF, and the coupling of the cysteine residue under standard conditions, the coupling of nonaoctanoic acid was performed in a DCM/DMF (1:1) mixture according to the previously described conditions. For deprotection and cleavage, the fully protected fragment was treated with TFA containing TIS (2.0%) and water (2.5%). The crude product was precipitated at 0 °C, washed several times with small portions of water, and recrystallized from methanol and water. The product was characterized by ^{1}H NMR spectroscopy and electrospray spectrometry.

C$_{18}$H$_{37}$CONHCysLys(DTPAGlu)CONH$_2$ (C18CysDT-PAGlu): ^{1}H MMR (chemical shifts δ, tetramethylsilane as the internal standard, DMSO-d_6 as the solvent) 4.4 (m, αCH Cys), 4.1 (m, 1H, αCH Lys), 3.5 (overlapped, 1H, αCH Glu), 3.3 (s, 8H, NCH$_2$COOH), 2.7–2.8 (m, 8H, RNCH$_2$CH$_2$NR), 2.14 (m 2H, C(O)CH$_2$CH$_2$R), 1.87 (m, γCH$_2$ Lys), 1.76 (m, 2H, δCH$_2$ Lys), 1.65 (m, 2H, βCH$_2$ Lys), 1.5 (overlapped, 2H, RCH$_2$CH$_3$), 1.1–1.3 (m, 30 H, 15 CH$_2$), 0.8 (t, 3H, 1 CH$_3$). [M + H]$^+$ = 976 amu (molecular weight 975).

The intramolecular disulfide bond reaction between the cysteine residues was carried out under the same conditions as described above in the case of C18CysL5CCK8, and the identity of the product was confirmed by LC-MS analysis.

[C$_{18}$H$_{37}$COCysLys(DTPAGlu)CONH$_2$]$_2$: R_t = 27.15 min; [M + H]$^+$ = 1,950 amu (molecular weight 1,949).

Preparation of gadolinium complexes

The preparation of gadolinium complexes was carried out by adding 2 equiv of GdCl$_3$ to an aqueous solution of the [C18CysDTPAGlu]$_2$ ligand at neutral pH and room temperature. The formation of the complexes was followed by measuring the solvent proton relaxation rate (1/T_1). The excess of uncomplexed Gd(III) ions, which yields a variation of the observed relaxation rate, was removed by filtering the complex solution left at pH 10 for 24 h with a 0.2-μm syringe filter, as already reported for other chelating amphiphilic monomers [11]. A xylenol orange UV-spectrophotometric method was used to check for the absence of free Gd(III) ions [31].

Solution preparation

Stock solutions of [C18CysDTPAGlu]$_2$, [C18CysDTPA-Glu(Gd)]$_2$, and [C18CysL5CCK8]$_2$ binary systems and [C18CysDTPAGlu]$_2$–[C18CysL5CCK8]$_2$ and [C18Cys-DTPAGlu(Gd)]$_2$–[C18CysL5CCK8]$_2$ ternary systems were prepared in 0.1 M phosphate buffer at pH 7.4. Solutions were stirred at room temperature until complete dissolution of the monomers and were then filtered through a 0.45-μm filter. All mixed solutions were prepared at 70:30 molar ratio between [C18CysDTPAGlu]$_2$ or [C18CysDTPA-Glu(Gd)]$_2$ and [C18CysL5CCK8]$_2$.

UV spectroscopy

The concentrations of solutions containing peptide surfactant were determined by absorbance measurement using a JASCO V-5505 UV–vis spectrophotometer equipped with a JASCO ETC.-505T Peltier temperature controller with a 1-cm quartz cuvette (Hellma). A molar absorptivity (ε_{280}) of 6,845 M^{-1} cm^{-1} was used for CCK8; this value was calculated according to the Edelhoch method [55], taking into account contributions from tyrosine and tryptophan present in the primary structure, which amount to 1,215 and 5,630 M^{-1} cm^{-1}, respectively [56].

Fluorescence spectroscopy

Cmc values of aggregates were obtained by fluorescence spectroscopy. Emission spectra were recorded at room temperature using a JASCO model FP-750 spectrofluorimeter in 1.0 cm path length quartz cell. Equal excitation and emission bandwidths were used throughout the experiments, with a recording speed of 125 nm min^{-1} and automatic selection of the time constant. The cmc values were measured by using ANS and pyrene as fluorescent probes. A stock solution of pyrene ($c = 1.0 \times 10^{-3}$ M) was prepared by adding a known weight of the compound to 20 wt% ethanol in water. The small amount of ethanol in the pyrene solution does not affect the spectral and self-aggregation behavior of amphiphiles. Small aliquots of 1×10^{-4} M aggregate solution, dissolved in 0.10 M phosphate buffer,

pH 7.4, were added to a fixed volume (1.00 mL) of fluorophore (1×10^{-5} M ANS or 2×10^{-6} M pyrene) directly in the quartz cell. In the ANS method, the cmc values were determined by linear least-squares fitting of the fluorescence at 480 nm, upon excitation at 350 nm versus the amphiphile concentration as previously reported [57, 58] In the pyrene method, the cmc values were determined from the break point of the fitting of I_1/I_3 upon excitation at 335 nm versus the amphiphile concentration.

Circular dichroism experiments

Far-UV CD spectra were collected at room temperature using a JASCO J-810 spectropolarimeter equipped with a NesLab RTE111 thermal controller unit using a 1-mm quartz cell. Other experimental settings were as follows: scan speed 10 nm min^{-1}; sensitivity 50 mdeg; time constant 16 s; bandwidth 3 nm. CD measurements were conducted on solutions containing peptide surfactant at concentrations of 1×10^{-4} M in 2.5 mM phosphate buffer at pH 7.4. The CD spectra were collected from 260 to 195 nm, corrected for the blank and adjusted for dilution. Thermal profiles (CD vs. temperature, in the 10–80 and 80–10 °C ranges) of the aggregates were recorded every 10 °C, with an equilibration time of 20 min for each measurement point. All samples were run in duplicate. The T_t was determined from the maximum of the first derivative of the heating and cooling curves.

Small angle neutron scattering measurements

SANS measurements were performed at various temperatures (in the 10–80 and 80–10 °C ranges) at the LOQ instrument sited at the ISIS facility of the Rutherford Appleton Laboratory (Chilton, UK). At the ISIS pulsed neutron source, the LOQ instrument uses neutrons of wavelengths ranging between 2.2 and 10 Å detected by a time-of-flight analysis on a 64-cm^2 two-dimensional detector placed 4.1 m from the sample [59], giving a q range of 0.006–0.24 Å^{-1}. Raw data were corrected for wavelength-dependent sample transmissions, incident spectrum, and detector efficiency and then put into absolute scattering cross sections $d\Sigma/d\Omega$ by comparison with scattering from a partially deuterated polystyrene standard. Samples were heated up from 10 to 80 °C at a rate of 1.0 °C min^{-1}, and cross sections were measured at 10, 40, 50, 60, and 80 °C. After that, they were cooled down at a rate of 1.0 °C min^{-1}, and cross sections were recorded at 50, 20, and 10 °C.

Water proton relaxation measurements

The longitudinal water proton relaxation rates were measured with a Stelar Spinmaster (Mede, Pavia, Italy)

spectrometer operating at 20 MHz, by means of the standard inversion-recovery technique (16 experiments, two scans). A typical 90° pulse width was 4 μs and the reproducibility of the T_1 data was ±0.5%. The temperature was maintained at 25 °C with a Stelar VTC-91 air-flow heater equipped with a copper-constantan thermocouple (uncertainty ±0.1 °C). The proton $1/T_1$ NMRD profiles were measured over a continuum of magnetic field strength from 0.00024 to 0.28 T (corresponding to 0.01–12 MHz proton Larmor frequency) using a Stelar fast field-cycling relaxometer. This relaxometer works under complete computer control with an absolute uncertainty in $1/T_1$ of ±1%. Data points at 20 and 90 MHz were added to the experimental NMRD profiles and were recorded with the Stelar Spinmaster (20 MHz) and with a JEOL (Tokyo, Japan) EX-90 (90 MHz) spectrometer, respectively.

^{17}O measurements

Variable-temperature ^{17}O NMR measurements were recorded at 2.1 T using the JEOL EX-90 spectrometer, equipped with a 5-mm probe, by using a D$_2$O external lock. The experimental settings were as follows: spectral width 10,000 Hz; 90° pulse (7 μs); acquisition time 10 ms; 1,000 scans; no sample spinning. Aqueous solutions containing 2.6% of the ^{17}O isotope (Yeda, Israel) were used. The observed transverse relaxation rates ($R_{2\text{obs}}^0$) were calculated from the signal width at half-height ($\Delta\nu_{i2} = R_{2\text{obs}}\pi\Delta\nu_{i2}$).

References

1. Caravan P, Ellison J, McMurry T, Lauffer R (1999) Chem Rev 99:2293–2352
2. Meade TJ, Taylor AK, Bull SR (2003) Curr Opin Neurobiol 13:597–602
3. Toth E, Helm L, Merbach AE (2001) The chemistry of contrast agents in medical magnetic resonance imaging, 1st edn. Wiley, London, pp 45–120
4. Aime S, Botta M, Fasano M, Terreno E (1998) Chem Soc Rev 27:19–29
5. Weinmann HJ, Mühler A, Radüchel B (2000) Methods in biomedical magnetic resonance. Imaging and spectroscopy. Wiley, Chichester
6. Banci L, Bertini I, Luchinat C (1991) Nuclear and electronic relaxation. VCH, Weinheim
7. Laus S, Sour A, Ruloff R, Toth E, Merbach AE (2005) Chem Eur J 11:3064–3076
8. Nasongkla N, Bey E, Ren J, Ai H, Khemtong C, Guthi JS, Chin S-F, Sherry AD, Boothman DA, Gao J (2006) Nano Lett 6:2427–2430

9. Dirksen A, Langereis S, de Waal BFM, van Genderen MHP, Hackeng TM, Meijer EW (2005) Chem Commun 2811–2813
10. Toth E, Bolskar RD, Borel A, Gonzalez G, Helm L, Merbach AE, Sitharaman B, Wilson LJ (2005) J Am Chem Soc 127:799–805
11. Accardo A, Tesauro D, Roscigno P, Gianolio E, Paduano L, D'Errico G, Pedone C, Morelli G (2004) J Am Chem Soc 126:3097–3107
12. Gløgård C, Stensrud G, Hovland R, Fossheim SL, Klaveness J (2002) Int J Pharm 233:131–140
13. Nasongkla N, Shuai X, Ai H, Weinberg BD, Pink J, Boothman DA, Gao J (2004) Angew Chem Int Ed 43:6323–6327
14. KingCP Li, Bednarski MD (2002) J Magn Reson Imaging 16:388–393
15. Reubi JC (2003) Endocr Rev 24:389–427
16. Accardo A, Tesauro D, Morelli G, Gianolio E, Aime S, Vaccaro M, Mangiapia G, Paduano L, Schillen K (2007) J Biol Inorg Chem 12:267–276
17. Tesauro D, Accardo A, Gianolio E, Paduano L, Teixeira J, Schillen K, Aime S, Morelli G (2007) Chembiochem 8:950–955
18. Vaccaro M, Mangiapia G, Paduano L, Gianolio E, Accardo A, Tesauro D, Morelli G (2007) Chemphyschem 8:2526–2538
19. Wank SA (1995) Am J Physiol Gastrointest Liver Physiol 269:G628–G646
20. Menger FM, Littau CA (1991) J Am Chem Soc 113:1451–1452
21. Zana R (2002) Adv Colloid Interface Sci 97:205–253
22. Jennings K, Marshall I, Birrell H, Edwards A, Haskins N, Sodermann O, Kirby AJ, Camilleri P (1998) Chem Commun 18:1951–1952
23. Camilleri P, Kremer A, Edwards AJ, Jennings KH, Jenkins O, Marshall I, McGregor C, Neville W, Rice SQ, Smith RJ, Wilkinson MJ, Kirby AJ (2000) Chem Commun 14:1253–1254
24. Ronsin G, Kirby AJ, Rittenhouse S, Woodnutt G, Camilleri PJ (2002) Chem Soc Perkin Trans 2:1302–1306
25. Lowik DW, Garcia-Hartjes J, Meijer JT, van Hest JCM (2005) Langmuir 21:524–526
26. Hamley IW, Ansari IA, Castelletto V, Nuhn H, Rosler A, Klok HA (2005) Biomacromolecules 6:1310–1315
27. Gorski N, Kalus J (2001) Langmuir 17:4211–4215
28. Bott R, Wolff T, Zierold K (2002) Langmuir 18:2004–2012
29. Chang WC, White PD (2000) Fmoc solid phase peptide synthesis. Oxford University Press, New York
30. Ellmann GL (1959) Arch Biochem Biophys 82:70–77
31. Barge A, Cravotto G, Gianolio E, Fedeli F (2006) Contrast Med Mol Imaging 1:184–188
32. Diwu Z, Lu Y, Zhang C, Klaubert DH, Haugland RP (1997) Photochem Photobiol 66:424–431
33. Menger FM (1979) Acc Chem Res 12:111–117
34. Zana R (2002) Langmuir 18(20):7759–7760
35. Menger FM, Jerkumica JM, Jhonston JC (1978) J Am Chem Soc 100:4676–4678
36. Mangiapia G, Accardo A, Lo Celso F, Tesauro D, Morelli G, Radulescu A, Paduano L (2004) J Phys Chem B 108:17611–17617
37. Underfriend S, Meienhofer J (1985) In: IHruby VJ (ed) The peptides, vol 7. Academic Press, New York
38. Pellegrini M, Mierke DF (1999) Biochemistry 38:14775–14783
39. Moroder L, D'Ursi A, Picone D, Amodeo P, Temussi PA (1993) Biochem Biophys Res Commun 190(3):741–746
40. Accardo A, Tesauro D, Mangiapia G, Pedone C, Morelli G (2007) Biopolymers 88:115–121
41. Radulescu A, Mathers RT, Coates GW, Richter D, Fetters L (2004) Macromolecules 37:6962–6971
42. Kotlarchyk M, Chen SH (1983) J Chem Phys 79:2461–2469
43. Nicolle GM, Toth E, Eisenwiener KP, Macke HR, Merbach AE (2002) J Biol Inorg Chem 7:757–769
44. Laus S, Sour A, Ruloff R, Toth E, Merbach AE (2005) Chem Eur J 11:3064–3076
45. Delli Castelli D, Gianolio E, Geninatti Crich S, Terreno E, Aime S (2008) Coord Chem Rev 252:2424–2443
46. Powell DH, Ni Dhubhghaill OM, Pubanz D, Helm L, Lebedev YS, Schlaepfer V, Merbach AE (1996) J Am Chem Soc 118:9333–9346
47. Aime S, Botta M, Fasano M, Terreno E (1999) Acc Chem Res 32:941–949
48. Lipari G, Szabo A (1982) J Am Chem Soc 104:4546–4559
49. Lipari G, Szabo A (1982) J Am Chem Soc 104:4559–4570
50. Nicolle GM, Helm L, Merbach AE (2003) Magn Reson Chem 41:794–799
51. Torchilin VP (2005) Nat Rev Drug Discov 4:145–154
52. Brandwijk RJMGE, Mulder WJM, Nicolay K, Mayo KH, Thijssen VLJL, Griffioen AW (2007) Bioconjug Chem 18:785–792
53. Reubi JC, Schaer JC, Waser B (1997) Cancer Res 57:1377–1386
54. Anelli PL, Fedeli F, Gazzotti O, Lattuada L, Lux G, Rebasti F (1999) Bioconjug Chem 10:137–140
55. Edelhoch H (1967) Biochemistry 6:1948–1954
56. Pace CN, Vajdos F, Fee L, Grimsley G, Gray T (1995) Protein Sci 4:2411–2423
57. Birdi KS, Singh HN, Dalsager SU (1979) J Phys Chem 83:2733–2737
58. De Vendittis E, Palumbo G, Parlato G, Bocchini V (1981) Anal Biochem 115:278–286
59. Heenan RK, Penfold J, King SM (1997) J Appl Crystallogr 30:1140–1147